B-5-4L

Extended Abstracts of the 2012 International Conference on Solid State Devices and Materials, Kyoto, 2012, pp620-621

Investigation of resistive switching mechanism and improved memory characteristics using IrO_x/high-κ_x/W structure

S. Maikap[1,*], W. Banerjee[1], B. L. You[1], D. Jana[1], H. Y. Lee[2], W. S. Chen[2], F. T. Chen[2], M. J. Kao[2], and M. J. Tsai[2]

[1]Thin Film Nano. Tech. Lab., Department of Electronic Engineering, Chang Gung University, Tao-Yuan, 333, Taiwan
[2]Electronics and Opto-Electronics Research Laboratories, Industrial Technology Research Institute, Hsinchu, 310, Taiwan
[*]Corresponding Author: Tel: 886-3-2118800 ext. 5785 Fax: 886-3-2118507 E-mail: sidhu@mail.cgu.edu.tw

1. Introduction

Recently, resistive switching memory (ReRAM) device is one of the promising candidates for future high-performance, low power consumption, and low cost nonvolatile memory applications [1-7]. Due to unknown switching mechanism and unstable switching, it is becoming bottleneck for applications in future. Most of the times, an initial formation is as essential process to have successive resistive hysteresis. But interestingly formation polarity has an important role to get impressive electrical characteristics. Formation polarity dependent ReRAM devices using high-κ_x AlO_x, GdO_x and HfO_x switching materials in a via structure with flat surface (FS) have been investigated and resistive switching mechanisms are also explained schematically based on electrical data. Furthermore, impact of nanodomes (NDs) in an IrO_x/AlO_x/W cross-point memory for the high-density 3D integration with an excellent uniformity, multi-level operation with low voltage operation of ±2V, low current compliance (I_{CC}) of <200 μA, low power of 10μW, and data retention at 85°C has also been reported.

2. Experiment

Firstly, a SiO_2 layer with a thickness of 200nm was grown by thermal oxidation on Si wafer. Next, 200nm thick tungsten (W) layer as a bottom electrode (BE) was deposited by RF sputter system for both via and cross-point type devices. Then, a SiO_2 layer with a thickness of 200 nm was deposited. Then, high-κ AlO_x, GdO_x and HfO_x materials were deposited on both via and cross-point structures. The BE surface was oxidized during deposition process and form WO_x layer. A layer of IrO_x (~200 nm) material as a top electrode (TE) was deposited by RF sputtering system. Finally, lift-off was performed to obtain the memory device.

3. Results and discussion

Fig.1 shows the current vs voltage (I-V) characteristics of the via type devices in IrO_x/high-κ_x/W structure with a CC of >500 μA. The I-V curve of the virgin devices and the hysteresis characteristics of the negative formation (NF) devices [Figs. 1(a), (c) & (e)] and the positive formation (PF) [Figs. 1(b), (d) & (f)] for the AlO_x, GdO_x and HfO_x based ReRAM devices are shown. After the formation process, the hysteresis switching direction is shown by arrows. Considering the electron affinities (χ) of 3.33, 1.25, 1.2 and 2.14 eV for WO_3, Al_2O_3, Gd_2O_3 and HfO_2 layers, respectively, the values of the effective barrier heights (Φ_b) are found to be [Φ_b= $(\Phi_m)_W$-$(\chi)_{WO3}$] 1.3 eV for the W/WO_x interface and [(Φ_b)= $(\Phi_m)_{IrOx}$-$(\chi)_{high\text{-}\kappa\ oxide}$] 3.95, 4.0, and 3.06 for the IrO_x/AlO_x, IrO_x/GdO_x and IrO_x/HfO_x interface, respectively. Therefore, the electron injection at the TE/high-κ_x will be lower than that of the BE/high-κ_x interface. The lower formation voltage of the PF devices have the ability to protect the device degradation as compare to the NF devices. Stable 100 consecutive DC switching cycles are observed for the high-κ PF devices as compare to the unstable 5 DC cycles of the NF devices. A higher RESET current is observed for the NF devices as compare to the PF devices owing to the current overshoot effect (Fig. 2). To rupture the filament, both oxidation and joule heating are responsible for the NF devices, while the oxidation is reponsible for the PF devices. For the NF devices, the LRS and HRS currents are fitted with ohmic and Schottky emission, respectively [Fig. 3(a)]. The oxygen deficient filaments formation is due to the oxygen ions (O^{2-}) migration from the high-κ_x layer toward the WO_x layer under SET [Fig. 4(a)]. The conducting filaments are ruptured randomly by oxidation under RESET [Fig. 4(b)], which shows unstable switching. On the other hand, both LRS and HRS currents are fitted linearly in log-log plot for the PF devices, which follows the TC-SCLC model [Fig. 3(b)]. The filament formation is also due to O^{2-} ions migration from the high-κ_x toward TE/high-κ_x interface under SET [Fig. 4(c)], which results a series oxygen-rich layer formation and limits the number of filament and diameter. Under RESET, the filament is oxidized at the oxygen-rich layer/filament interface, resulting in a reduction of random ruptured of the filaments as well as repeatable switching is observed [Fig. 4(d)]. To improve further the resistive switching characteristics, a cross-point memory in an IrO_x/AlO_x/W structure with NDs on the BE is designed for the PF devices [Fig. 5(a)]. Schematic view [Fig. 5(b)] and HRTEM image [Fig. 5(c)] of the cross-point memory with a tip ND diameter of ~3 nm are shown. Fig. 6 shows excellent repeatable 1000 consecutive I-V hysteresis switching cycles with a current compliance (I_{CC}) of 200μA and an small operation voltage of ±2V. The applicable SET voltage +1V is observed. This cross-point device is formation free because of the defects within percolation length. All devices show an excellent switching with a resistance ratio (HRS/LRS) of $>10^2$. The filament formation [Fig. 7(a)] and rupture [Fig. 7(b)] are controlled and confined by the tip of the ND because of high electric field on the tip of ND. Fig. 8 shows the statistical distribution of different levels for the LRS (controlled by I_{CC} of 50-200 μA) and HRS (controlled by stop voltage, V_{STOP} of -1.2 to -2.0 V). Clearly identified LRS [Fig. 9(a)] and HRS [Fig. 9(b)] of 10^4 cycles with I_{CC} values from 10μA to 200μA and V_{STOP} values from -1.2V to -2.0V, with well defined sensing window are obtained. Fig. 9(c) shows a very good >40k AC cycles of the devices at the I_{CC} of 200μA. Fig. 9 shows the retention at 85°C for the NF and PF devices with AlO_x layer. Fig. 10 shows excellent data retention of $>10^4$s for the cross-point resistive switching memory devices with different levels of LRS [Fig. 10(a)] and HRS [Fig. 10(b)] at 85°C.

4. Conclusion

High-κ_x (HfO_x, GdO_x, and AlO_x) oxide based formation-polarity-dependent resistive switching mechanism and improved memory performance of cross-point resistive switching memory devices are investigated for the first time. Oxygen ion migration and controlled migration by series oxygen-rich layer and nanodomes are the key points to improve the memory performance in an IrO_x/high-k_x/W structure. Very stable resistance switching behaviors with a long endurance of >40k cycles, excellent retention at 85°C, MLC operation in both LRS and HRS with small operation voltage of ±2V and an I_{CC} of <200 μA are achieved. The cross-point memory device can be operated with a low current of 10 μA for future nanoscale non-volatile memory with 3D integration.

Acknowledgment

Thanks a lot to National Science Council (NSC), Taiwan, under contract no. NSC-101-2221-E-182-061 to support this research work.

References

[1] A. Sawa, Mater. Today, vol. 11, p. 28, 2008. [2] R. Waser et al., Advanced Mat. vol. 21, p. 2632, 2009. [3] J. J. Yang et al., Appl. Phys. Lett., vol. 92, pp. 232102, 2010. [4] H.Y. Lee et al., Electron Dev. Lett., vol. 31, pp. 44-46, 2010. [5] C. P. Hsiung et al., ACS Nano, 4, 5414 (2010). [6] W. Banerjee et al., J. Electrochem. Soc., vol. 159, p. H1, 2011. [7] W. Banerjee et. al., Jpn. J. Appl. Phys, vol. 51, 04DD10, 2012.

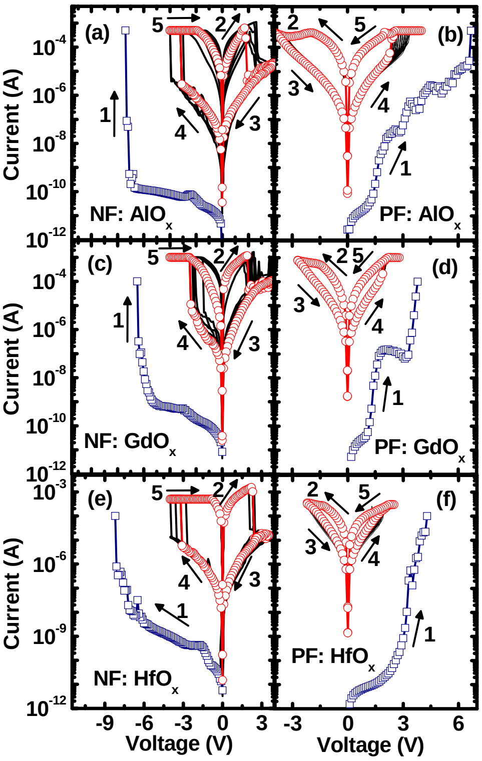

Fig. 1. Typical I-V hysteresis characteristics of (a) NF: AlO_x, (b) PF: AlO_x, (c) NF: GdO_x, (d) PF: GdO_x, and (e) NF: HfO_x, (f) PF: HfO_x memory device for the via structures.

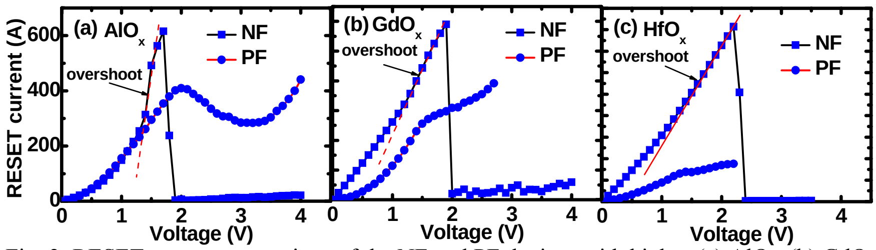

Fig. 2. RESET current comparison of the NF and PF devices with high-κ (a) AlO_x, (b) GdO_x and (c) HfO_x in via structures. Higher RESET current can be observed for the NF devices as compare to that of the PF devices, which can degrade the device performance.

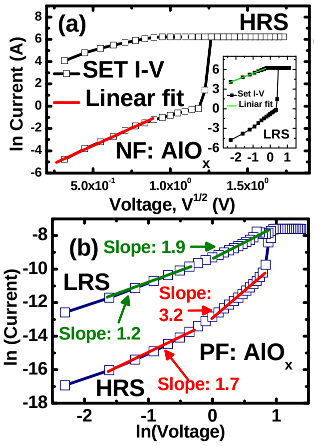

Fig. 3. (a) Schottky fit of HRS and ohmic of LRS (inset) for NF and (b) TC-SCLC for PF device.

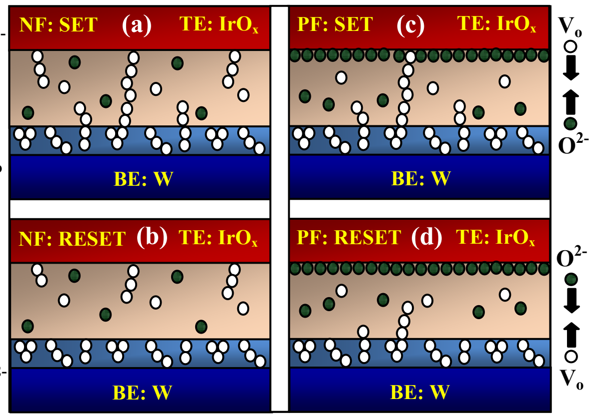

Fig. 4. Schematic switching mechanisms of NF device **(a)** SET, **(b)** RESET, and **(c)** SET and **(d)** RESET for PF device. The controlled O^{2-} ions migration of the PF device is playing the key role to improve device performance.

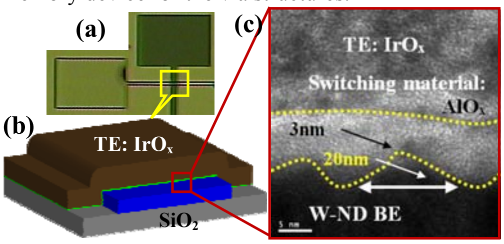

Fig. 5. **(a)** Optical image of 1×1 point, **(b)** illustration of a single cross-point memory with AlO_x as a switching material. **(c)** HRTEM image of W-ND formation at BE.

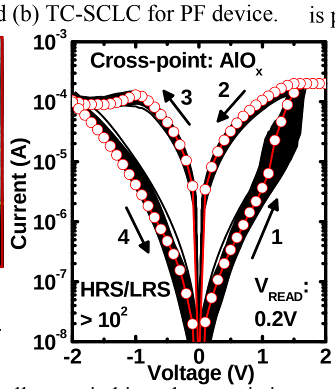

Fig. 6. Excellent switching characteristics with 1000 consecutive cycles. A high resistance ratio of >100 is observed.

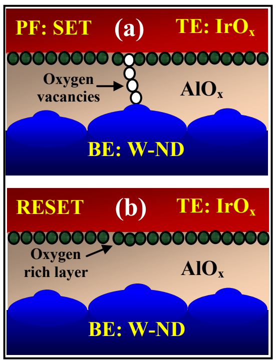

Fig. 7. Schematic mechanisms under the **(a)** SET and **(b)** RESET operations.

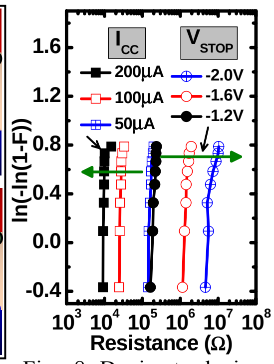

Fig. 8 Device-to-device Weibull distribution with MLC at LRS and HRS.

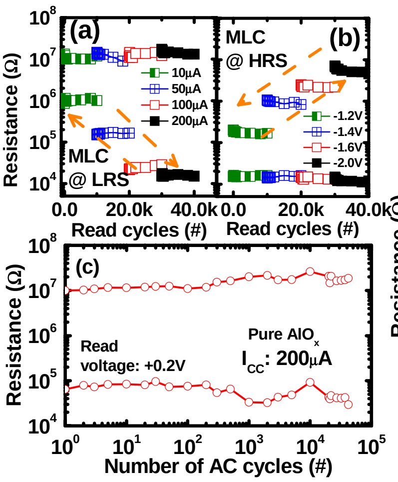

Fig. 8. Read immunity measurement with MLC at (a) LRS and (b) HRS of 10^4 cycles at each level. (c) Excellent endurance > 40000 AC cycles.

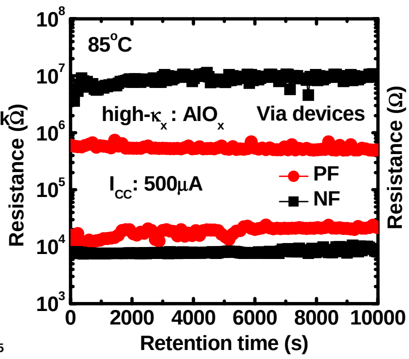

Fig. 9. Retention characteristics of the high-κ AlO_x based via devices for the NF and PF conditions. LRS of the PF devices goes slightly higher after 10^4s of retention.

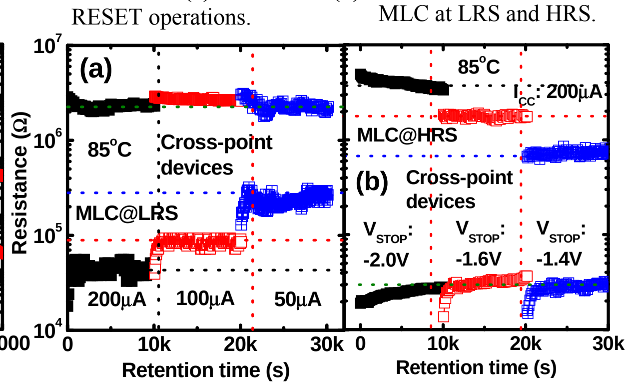

Fig. 10. (a) Devices are capable to show the data retention at 85°C with a low power of 50μW. (b) Fixed LRS can be observed with distinguishable HRS at different V_{STOP} values. Retention at each level was measured for 10^4 s of retention time at 85°C.